Diffusive to Nonergodic Dipolar Transport in a Dissipative Atomic Medium

S. Whitlock,[1,2,*] H. Wildhagen,[1] H. Weimer,[3] and M. Weidemüller[1,4]
[1]Physikalisches Institut, Universität Heidelberg, Im Neuenheimer Feld 226, 69120 Heidelberg, Germany
[2]IPCMS (UMR 7504) and ISIS (UMR 7006), Université de Strasbourg and CNRS, 67000 Strasbourg, France
[3]Institut für Theoretische Physik, Leibniz Universität Hannover, Appelstraße 2, 30167 Hannover, Germany
[4]Hefei National Laboratory for Physical Sciences at the Microscale and Department of Modern Physics, and CAS Center for Excellence and Synergetic Innovation Center in Quantum Information and Quantum Physics, University of Science and Technology of China, Hefei, Anhui 230026, China

(Received 20 September 2018; published 22 November 2019)

We investigate the dipole-mediated transport of Rydberg impurities through an ultracold gas of atoms prepared in an auxiliary Rydberg state. In one experiment, we continuously probe the system by coupling the auxiliary Rydberg state to a rapidly decaying state that realizes a dissipative medium. *In situ* imaging of the impurities reveals diffusive spreading controlled by the intensity of the probe laser. By preparing the same density of hopping partners, but then switching off the dressing fields, the spreading is effectively frozen. This is consistent with numerical simulations, which indicate the coherently evolving system enters a nonergodic extended phase. This opens the way to study transport and localization phenomena in systems with long-range hopping and controllable dissipation.

DOI: 10.1103/PhysRevLett.123.213606

The transport of charge, energy, or information plays a fundamental role in science and technology, for example, determining the function of nanoelectronic devices [1], photochemical and biophysical processes [2], and even the dynamics of complex networks [3]. Usually, however, the relevant transport mechanisms depend very strongly on the underlying structure of each system and its coupling to the environment. For example, in disordered systems governed by short-range hopping, transport can be exponentially suppressed due to Anderson localization [4,5] or many-body localization [6,7]. In contrast, long-range hopping or decoherence introduced by coupling to a dissipative environment tends to destroy localization effects. Comparatively little is known about the interface between short- and long-range hopping (e.g., dipolar $1/r^3$ hopping in three dimensions) [8–13] or systems situated at the quantum-classical crossover [14–17], which are of special interest for discovering and understanding new transport mechanisms.

In this Letter, we report an experimental and theoretical study of the transport of atomic excitations in a three-dimensional ultracold atomic gas governed by dipolar hopping interactions and subject to a controllable dissipative environment. We start with a small number of Rydberg excitations in a Rydberg np state ("impurities") embedded in a gas of atoms prepared in an auxiliary Rydberg ns state ("background"). The huge dipole moments of highly excited Rydberg states lead to coherent energy exchange between np and ns states, allowing the impurities to migrate through the gas of ns atoms that acts as a medium [18–31]. By additionally coupling the ns states to short-lived spontaneously decaying states via laser fields, we can spatially resolve the impurity atoms [29,32]. Fundamentally different transport behavior is observed when the probe laser is on continuously (thereby continuously watching the dynamics) or when the system is allowed to evolve in the absence of laser fields. We show that the diffusion rate can be controlled through the intensity of the probe laser and in the limit of zero intensity the diffusion stops completely. Supporting numerical simulations suggest the likely explanation is the system entering a nonergodic extended phase linked to dipolar hopping and disorder. This realizes a platform for studying and controlling transport and localization phenomena in classical and quantum regimes, complementary to other experimental platforms involving ground-state atoms [33–40], trapped ions [41–44], photonic networks [45–47], and superconducting qubits [48,49], with excellent control concerning disorder, dimensionality, dissipation, and long-range interactions.

We begin our experiments by preparing 10^4 ^{87}Rb atoms in a cigar-shaped optical trap with a temperature of 40 μK [Fig. 1(a)]. The cloud has an elongated Gaussian shape with $e^{-1/2}$ radii of $\{12, 12, 200\}$ μm and a peak density of ground-state atoms of 0.1 μm^{-3}. On the relevant timescale of our experiments (a few tens of microseconds), the atoms are effectively frozen in space such that dynamics only occurs in the internal (Rydberg) state degrees of freedom. The basic processes involved to study transport in our experiment are illustrated in Fig. 1(b). We first create a small number of impurity Rydberg excitations in the $|n's = 50s_{1/2}\rangle$ state by switching off the optical trap and

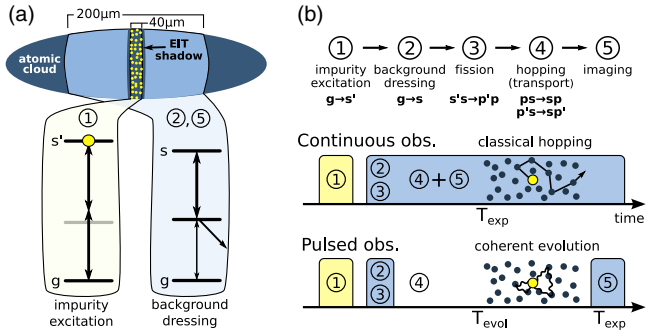

FIG. 1. Setup for studying dipolar-mediated excitation transport in a controllable dissipative medium. (a) Sketch of the experimental geometry and level scheme used to prepare the Rydberg impurities and background gas and to observe transport. (b) The experimental sequence starts exciting a small number of impurities at the center of an ultracold atomic gas. We then couple a larger volume of atoms to a second Rydberg state via an EIT resonance. The presence of impurities is signaled by increased absorption on the probe laser. Different transport behavior is observed depending on whether the probe laser is left on continuously or pulsed.

then applying a two-photon laser excitation, which illuminates a strip of approximately 40 μm width at the center of the cloud [Fig. 1(a)]. Following this, we couple a larger region of approximately 200 μm width using a second set of lasers on an electromagnetically induced transparency (EIT) resonance in ladder configuration $|5s_{1/2}\rangle \rightarrow |5p_{3/2}\rangle \rightarrow |ns = 48s_{1/2}\rangle$. This involves a strong coupling laser with Rabi frequency $\Omega_c/2\pi = 7.2$ MHz (upper transition) and a weaker probe laser with variable Rabi frequency Ω_p (lower transition). The spontaneous decay rate of the intermediate state is $\Gamma/2\pi = 6.1$ MHz.

In the absence of impurities, the EIT coupling renders the cloud partly transparent and establishes a small steady-state fraction of Rydberg excitations in the $|ns\rangle$ state, corresponding to a mean inter-Rydberg distance of 8.5 μm. The specific Rydberg states used were chosen because of the near degeneracy of the $|ns, n's\rangle \leftrightarrow |np = 48p_{1/2}, n'p = 49p_{1/2}\rangle$ pair states. As a result, within approximately 1 μs each impurity excitation is converted into two np, $n'p$ excitations (fission), which can then migrate through the remaining background gas via resonant exchange processes such as $|ns, np\rangle \leftrightarrow |np, ns\rangle$ and $|ns, np'\rangle \leftrightarrow |np', ns\rangle$. Crucially, these interactions cause fast hopping of excitations on the μs timescale and with dipolar character (hopping rate scaling as $1/r^3$ with the interatomic distance). The lifetimes of the np, $n'p$ states including blackbody decay are $\approx$80 μs, such that the impurities persist over timescales much longer than the hopping dynamics. In our experiments, the ns, np and ns, $n'p$ interactions are almost the same (interaction coefficient $C_3/2\pi \approx 5.2$ GHz μm^3) and as such we do not distinguish between np or $n'p$ impurities.

To monitor the ensuing dynamics we make use of the interaction-enhanced-imaging technique, which uses the background atoms as an amplifying medium for detecting impurity atoms [29,32]. In the absence of impurities, the atomic gas is mostly transparent for the probe laser due to EIT. However, in the vicinity of each impurity, the strong dipolar interactions shift the excited state out of resonance, thereby breaking the EIT condition for the background gas atoms and locally increasing the photon scattering rate to $R_{sc} \approx \Omega_p^2/(2\Gamma)$, which can be varied over the range $R_{sc}/2\pi \lesssim 500$ kHz. To observe the spatial distribution of impurities the transmitted probe light is imaged onto a CCD camera. Because of the relatively fast Rydberg hopping dynamics, the camera effectively integrates this signal from the start of the dynamics up to the exposure time T_{exp} [Fig. 1(b)]. By subtracting images of the probe light taken with and without impurities, we recover a two-dimensional image that we integrate over the radial coordinate as shown in Figs. 2(a) and 2(b).

To explore both incoherent and coherent transport regimes, we perform two different types of experiments. In experiment 1, the probe laser is kept on continuously, leading to a continuous spatial measurement of the time-integrated impurity distribution. In experiment 2, we use a pulsed observation scheme in which we trigger the dynamics with a short probe pulse to prepare a medium with the same density of $|s\rangle$ excitations and then let the system evolve without a probe light for a variable time. Afterwards a second probe pulse is applied to spatially resolve the final distribution of impurity atoms.

Experiment 1: Continuous observation.—The continuous spatial projection of the positions of the impurities due to the probe light leads to classical diffusive transport. To demonstrate this, Fig. 2(a) shows a density plot of the impurity distribution as a function of time. This is compared to a solution of the classical diffusion law $\dot{n}(x,t) = D\partial^2 n(x,t)/\partial x^2$. The experiment clearly shows that the impurities spread through the atomic medium, with the spatial distribution increasing in width by a factor of 3 within 15 μs. The experimentally determined distributions are in excellent agreement with the solution to the diffusion law for an initial Gaussian density distribution with fitted width $\sigma(t = 0) = 17(1)$ μm and diffusion constant $D = 84(3)$ μm$^2/\mu$s [also shown in Fig. 2(a)], where the uncertainties indicated in parentheses are obtained by bootstrap resampling of the full spatiotemporal dataset used for fitting. Taking into account that the signal is averaged over the variable exposure time on the camera, we expect the true diffusion rate is a factor of 2 larger than deduced from the time-integrated spatial distributions [29]. The diffusive nature of the transport is further evident in the second central moment $\langle x(t)^2\rangle = \int x^2 n(x,t)dx/\int n(x,t)dx$ of the measured impurity distribution, which grows linearly in time [squares in Fig. 2(c)].

Crucially, the observed diffusion rate can be controlled by the EIT laser fields used to create the dissipative medium. As the intensity of the probe laser field is varied,

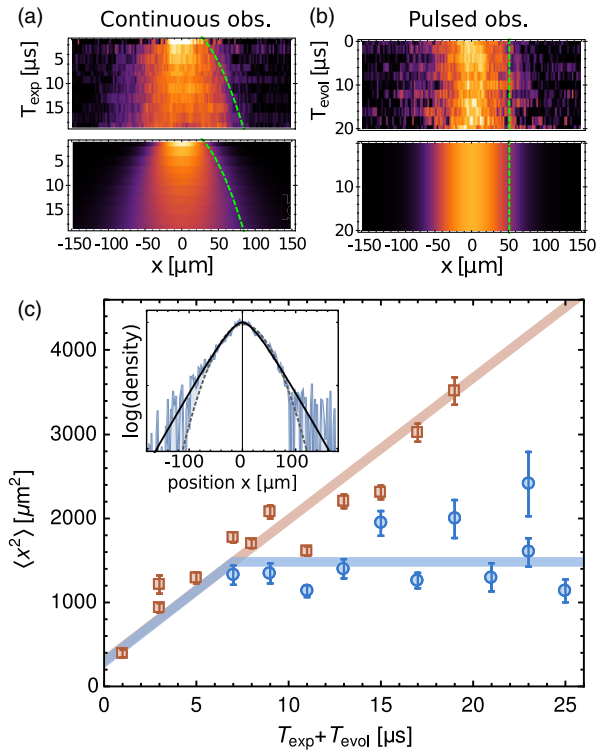

FIG. 2. Transport of Rydberg impurities under continuous and pulsed observation. (a) Density plots of the spatial distribution of impurities along the axial x direction as a function of time under continuous observation for $R_{sc}/2\pi = 250$ kHz. (Upper) The experimental measurements. (Lower) Corresponds to the solution to the classical diffusion law. (b) Corresponding density plots for the case of pulsed observation showing the absence of diffusion. (Lower) Gaussian distribution determined by the preparation and probe periods with no dynamics during the evolution period. The dotted green lines in (a) and (b) depict the time-dependent widths of the distribution from the respective time-evolution model. (c) Measured mean square deviation $\langle x^2 \rangle$ as a function of the total time, which is the sum of the free evolution time and the exposure time for imaging. The solid lines are fits to the diffusion law showing diffusive (linear) and frozen (constant) dynamical evolution. (Inset) The stationary density profile obtained averaging the data shown in (b). The dashed line shows a fit to a Gaussian distribution and the solid black line shows a fit to Gaussian with exponential wings expected from theory.

we anticipate two effects: First, the density of hopping partners is modified due to the dependence of the Rydberg ns state admixture on the ratio of probe and coupling laser intensities. Second, the rate of decoherence induced by the continuous measurement process changes with the photon scattering rate. A theoretical model that takes both effects into account in the weak probe limit predicts that the classical hopping rate, and thus the diffusion rate, should scale proportional to the probe laser intensity [25]. To test this prediction, we measured the diffusion rate for a fixed exposure time of $T_{exp} = 21$ μs as a function of probe intensity, expressed in terms of the square of the probe Rabi

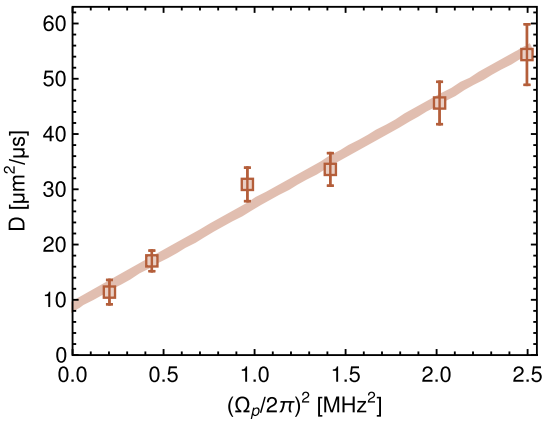

FIG. 3. Linear dependence of the diffusion coefficient of the dissipative medium on the squared probe Rabi frequency Ω_p.

frequency in Fig. 3. The data are consistent with the predicted proportional intensity dependence. However, in contrast to the assumption of simple diffusive transport, we find a minimum diffusion rate of $9(2)$ $\mu m^2/\mu s$ (obtained for $\Omega_p \to 0$). This rate is too large to be explained by thermal motion of the impurity atoms and instead might be evidence for a crossover to coherent transport when the photon scattering rate becomes small compared to the coherent hopping rate, which is further investigated in the next section.

Experiment 2: Pulsed observation.—We now explore the transport properties of the Rydberg medium in the absence of the dissipative environment. As in the previous experiments, we prepare impurities in state $|n's\rangle$. This is then followed by the application of the EIT lasers for approximately 2 μs, where the coupling laser is switched off 500 ns before the probe laser. This establishes the background medium with the same density of $|ns\rangle$ Rydberg excitations as in experiment 1 and triggers the fission process. We confirm that the initial conditions for experiments 1 and 2 are equivalent by the fact that the width of the impurity distribution after this pulse measured with a 5 μs exposure time matches the continuous observation case for $T_{exp} = 7$ μs [Fig. 2(c)] and that the number of ns atoms in the gas measured by field ionization detection remains unchanged during and after the excitation pulse. After this preparation phase, we allow the system to evolve in the absence of probe and coupling light for a variable time T_{evol}. This is then followed by a final 5 μs long imaging pulse.

Figure 2(c) compares the case of pulsed observation (circles) to that of the continuous observation (squares) as a function of the integrated evolution and probe laser exposure times. For pulsed observation, we observe a time dependence that is consistent with a total freezing of the hopping dynamics beyond what can be explained by classical diffusion during the preparation and imaging pulses [Figs. 2(b) and 2(c)]. This is suggestive of localizationlike behavior on the dipolar hopping dynamics.

To explain these observations, we perform numerical simulations assuming purely coherent evolution under the dipolar hopping Hamiltonian $H = \sum_{ij} C_3/r_{ij}^3 |ns\rangle_i |np\rangle_j \langle np|_i \langle ns|_j + \text{H.c.}$ This model also maps to a tight-binding-type model, where an np excitation acts like a "particle" that is free to hop to any other site (ns excitations) with a probability weighted by a power law in the distance. We randomly place up to 16 000 background Rydberg atoms (sites) in a three-dimensional elongated volume comparable to the experiment, including a constraint to satisfy Rydberg blockade effects between nearby atoms. Additionally, we limit ourselves to the single impurity subspace, i.e., equivalent to neglecting interactions between the impurities. The simulations start with the impurity excitation localized on a central atom, which is then evolved according to the time-dependent Schrödinger equation. Finally, we extract the spatial probability distribution for the impurity excitation as a function of time, averaging over many disorder realizations. Generally, the simulations show a period of rapid spreading over a timescale of approximately 1 μs, which then freezes, leaving an approximately exponential probability distribution.

To test this theoretical prediction, we subsequently analyzed the stationary spatial distribution of impurity atoms shown in Fig. 2(b). The inset to Fig. 2(c) shows the measured average distribution on a log-linear scale. To improve the signal-to-noise ratio in the wings, we subtract the background absorption using the methods described in Ref. [50] and average over all the data for $T > 7$ μs, corresponding to 1600 runs of the experiment. The center of the distribution can be described by a Gaussian function according to the previously measured diffusion law given the total probe exposure time (dashed line in the inset). However the data also suggest a small deviation from a Gaussian in the wings, which resemble the exponential tails seen in the theoretical simulations (seen by the fit to a Gaussian distribution with exponential tails, solid black line), although these wings are slightly less pronounced than predicted. This might hint at effects beyond the coherent dipolar hopping dynamics of independent impurities. A quantitative comparison between experiment and theory is complicated by diffusive dynamics during the probing phase, which is currently not included in the theory.

Within the numerical simulations, we can now investigate the cause for the absence of spreading observed in the experiment. For this we perform a finite size scaling of the higher order moments $I_q = \sum_j |\psi(j)|^{2q}$, where ψ refers to the single particle eigenstates of the dipolar hopping Hamiltonian and the index j runs over all atoms. Here, we focus on an average of I_q restricted to eigenstates at the center of the band, as these play the dominant role in the experimental setting. For the finite size scaling, we keep the density and aspect ratio at fixed values. Generically, I_q will scale as a power law $I_q \sim N^{D_q(1-q)}$ with N being the number of sites [51]. The fractal dimension D_q can be used to classify the transport behavior for the system: $D_q = 0$ signals the presence of localization, while states with finite D_q are extended. However, deviations from $D_q = 1$ signal the presence of nonergodic extended states [51].

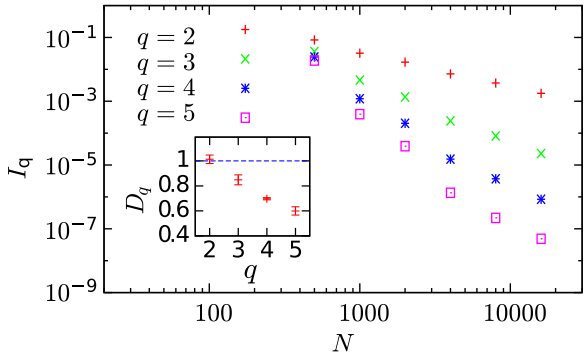

FIG. 4. Numerical simulations of the dipolar hopping Hamiltonian showing the inverse participation ratio and fractal dimension at late times as a function of the system size assuming purely coherent evolution under dipolar exchange interactions. Different symbols correspond to the moments I_q of the wave function defined in the text. (Inset) Fractal dimension D_q as a function of q obtained from power law fits to I_q for large system sizes. The solid line corresponds to $D_q = 1$ for ergodic states.

Indeed, from the finite size scaling of I_q, we find a significant reduction of the fractal dimension D_q for $q > 2$, but still well above zero, see Fig. 4. This breaking of ergodicity is the likely explanation for the dramatic reduction of the spreading as compared to the diffusive case, despite the $1/r^3$ hopping that is expected to break localization in 3D [8–13]. We note that this finding is in agreement with other simulations for dipolar transport in disordered lattice models [10].

In conclusion, we have studied the dipolar energy transport dynamics in Rydberg gases both in a dissipative medium and under purely coherent dynamics. In the first case, we observe dynamics characteristic of classical diffusion with a tunable diffusion coefficient. In the case of pulsed observation, we find that the spreading of impurities is effectively frozen, which we attribute to the system entering a nonergodic phase. These experiments establish Rydberg excitations as a unique platform to study quantum transport, including novel regimes arising as a consequence of long-range interactions. Our experiments, combined with the high degree of flexibility afforded by ultracold gases to control the spatial geometry, types of disorder, range of interactions, and degree of coherence, pave the way for future studies addressing important outstanding questions on many-body localization, nonequilibrium phase transitions, and the dynamics of nonergodic extended states.

We thank J. Evers, X. Deng, G. Pupillo, and L. Santos for fruitful discussions as well as G. Günter and V. Gavryusev for contributions to the experimental apparatus.

This work is part of and supported by the DFG Collaborative Research Centres "SFB 1225 (ISOQUANT)" and "SFB 1227 (DQ-mat)," the Priority Programme DFG SPP 1929 GiRyd, the Heidelberg Center for Quantum Dynamics, the European Union H2020 FET Proactive project RySQ (Grant No. 640378) and the "Investissements d'Avenir" programme through the Excellence Initiative of the University of Strasbourg (IdEx). S. W. was partially supported by the University of Strasbourg Institute for Advanced Study (USIAS) and H. W. acknowledges support by the Volkswagen Foundation.

*whitlock@unistra.fr

[1] S. Datta, *Lessons from Nanoelectronics: A New Perspective on Transport* (World Scientific, Singapore, 2017).
[2] G. D. Scholes, G. R. Fleming, A. Olaya-Castro, and R. van Grondelle, Lessons from nature about solar light harvesting, Nat. Chem. **3**, 763 (2011).
[3] O. Mülken and A. Blumen, Continuous-time quantum walks: Models for coherent transport on complex networks, Phys. Rep. **502**, 37 (2011).
[4] P. W. Anderson, Absence of diffusion in certain random lattices, Phys. Rev. **109**, 1492 (1958).
[5] P. A. Lee and T. V. Ramakrishnan, Disordered electronic systems, Rev. Mod. Phys. **57**, 287 (1985).
[6] D. M. Basko, I. L. Aleiner, and L. Altshuler, Metal–insulator transition in a weakly interacting many-electron system with localized single-particle states, Ann. Phys. (Amsterdam) **321**, 1126 (2006).
[7] I. V. Gornyi, A. D. Mirlin, and D. G. Polyakov, Interacting Electrons in Disordered Wires: Anderson Localization and Low-t Transport, Phys. Rev. Lett. **95**, 206603 (2005).
[8] J. Eisert, M. van den Worm, S. R. Manmana, and M. Kastner, Breakdown of Quasilocality in Long-Range Quantum Lattice Models, Phys. Rev. Lett. **111**, 260401 (2013).
[9] N. Y. Yao, C. R. Laumann, S. Gopalakrishnan, M. Knap, M. Müller, E. A. Demler, and M. D. Lukin, Many-Body Localization in Dipolar Systems, Phys. Rev. Lett. **113**, 243002 (2014).
[10] X. Deng, B. L. Altshuler, G. V. Shlyapnikov, and L. Santos, Quantum Levy Flights and Multifractality of Dipolar Excitations in a Random System, Phys. Rev. Lett. **117**, 020401 (2016).
[11] Z. Eldredge, Z.-X. Gong, J. T. Young, A. Hamed Moosavian, M. Foss-Feig, and A. V. Gorshkov, Fast Quantum State Transfer and Entanglement Renormalization Using Long-Range Interactions, Phys. Rev. Lett. **119**, 170503 (2017).
[12] X. Deng, V. E. Kravtsov, G. V. Shlyapnikov, and L. Santos, Duality in Power-Law Localization in Disordered One-Dimensional Systems, Phys. Rev. Lett. **120**, 110602 (2018).
[13] G. A. Álvarez, D. Suter, and R. Kaiser, Localization-delocalization transition in the dynamics of dipolar-coupled nuclear spins, Science **349**, 846 (2015).
[14] M. B. Plenio and S. F. Huelga, Dephasing-assisted transport: Quantum networks and biomolecules, New J. Phys. **10**, 113019 (2008).
[15] P. Rebentrost, M. Mohseni, I. Kassal, S. Lloyd, and A. Aspuru-Guzik, Environment-assisted quantum transport, New J. Phys. **11**, 033003 (2009).
[16] A. W. Chin, A. Datta, F. Caruso, S. F. Huelga, and M. B. Plenio, Noise-assisted energy transfer in quantum networks and light-harvesting complexes, New J. Phys. **12**, 065002 (2010).
[17] R. J. Bettles, J. Minář, C. S. Adams, I. Lesanovsky, and B. Olmos, Topological properties of a dense atomic lattice gas, Phys. Rev. A **96**, 041603(R) (2017).
[18] W. R. Anderson, J. R. Veale, and T. F. Gallagher, Resonant Dipole-Dipole Energy Transfer in a Nearly Frozen Rydberg Gas, Phys. Rev. Lett. **80**, 249 (1998).
[19] I. Mourachko, D. Comparat, F. de Tomasi, A. Fioretti, P. Nosbaum, V. M. Akulin, and P. Pillet, Many-Body Effects In a Frozen Rydberg Gas, Phys. Rev. Lett. **80**, 253 (1998).
[20] O. Mülken, A. Blumen, T. Amthor, C. Giese, M. Reetz-Lamour, and M. Weidemüller, Survival Probabilities in Coherent Exciton Transfer with Trapping, Phys. Rev. Lett. **99**, 090601 (2007).
[21] T. Scholak, F. de Melo, T. Wellens, F. Mintert, and A. Buchleitner, Efficient and coherent excitation transfer across disordered molecular networks, Phys. Rev. E **83**, 021912 (2011).
[22] S. Wüster, C. Ates, A. Eisfeld, and J.-M. Rost, Excitation transport through Rydberg dressing, New J. Phys. **13**, 073044 (2011).
[23] F. Robicheaux and N. M. Gill, Effect of random positions for coherent dipole transport, Phys. Rev. A **89**, 053429 (2014).
[24] D. W. Schönleber, A. Eisfeld, M. Genkin, S. Whitlock, and S. Wüster, Quantum Simulation of Energy Transport with Embedded Rydberg Aggregates, Phys. Rev. Lett. **114**, 123005 (2015).
[25] H. Schempp, G. Günter, S. Wüster, M. Weidemüller, and S. Whitlock, Correlated Exciton Transport in Rydberg-Dressed-Atom Spin Chains, Phys. Rev. Lett. **115**, 093002 (2015).
[26] W. R. Anderson, M. P. Robinson, J. D. D. Martin, and T. F. Gallagher, Dephasing of resonant energy transfer in a cold Rydberg gas, Phys. Rev. A **65**, 063404 (2002).
[27] S. Westermann, T. Amthor, A. L. de Oliveira, J. Deiglmayr, M. Reetz-Lamour, and M. Weidemüller, Dynamics of resonant energy transfer in a cold Rydberg gas, Eur. Phys. J. D **40**, 37 (2006).
[28] C. S. E. van Ditzhuijzen, A. F. Koenderink, J. V. Hernández, F. Robicheaux, L. D. Noordam, and H. B. van Linden van den Heuvell, Spatially Resolved Observation of Dipole-Dipole Interaction Between Rydberg Atoms, Phys. Rev. Lett. **100**, 243201 (2008).
[29] G. Günter, H. Schempp, M. Robert-de Saint-Vincent, V. Gavryusev, S. Helmrich, C. S. Hofmann, S. Whitlock, and M. Weidemüller, Observing the dynamics of dipole-mediated energy transport by interaction-enhanced imaging, Science **342**, 954 (2013).
[30] S. Ravets, H. Labuhn, D. Barredo, L. Béguin, T. Lahaye, and A. Browaeys, Coherent dipole-dipole coupling between two single atoms at a Förster resonance, Nat. Phys. **10**, 914 (2014).

[31] D. Barredo, H. Labuhn, S. Ravets, T. Lahaye, A. Browaeys, and C. S. Adams, Coherent Excitation Transfer in a Spin Chain of Three Rydberg Atoms, Phys. Rev. Lett. **114**, 113002 (2015).

[32] G. Günter, M. Robert-de-Saint-Vincent, H. Schempp, C. S. Hofmann, S. Whitlock, and M. Weidemüller, Interaction Enhanced Imaging of Individual Rydberg Atoms in Dense Gases, Phys. Rev. Lett. **108**, 013002 (2012).

[33] E. Akkermans, A. Gero, and R. Kaiser, Photon Localization and Dicke Superradiance in Atomic Gases, Phys. Rev. Lett. **101**, 103602 (2008).

[34] G. Roati, C. D'Errico, L. Fallani, M. Fattori, C. Fort, M. Zaccanti, G. Modugno, M. Modugno, and M. Inguscio, Anderson localization of a non-interacting Bose–Einstein condensate, Nature (London) **453**, 895 (2008).

[35] J. Billy, V. Josse, Z. Zuo, A. Bernard, B. Hambrecht, P. Lugan, D. Clément, L. Sanchez-Palencia, P. Bouyer, and A. Aspect, Direct observation of Anderson localization of matter waves in a controlled disorder, Nature (London) **453**, 891 (2008).

[36] S. S. Kondov, W. R. McGehee, J. J. Zirbel, and B. DeMarco, Three-dimensional Anderson localization of ultracold matter, Science **334**, 66 (2011).

[37] S. Krinner, D. Stadler, D. Husmann, J.-P. Brantut, and T. Esslinger, Observation of quantized conductance in neutral matter, Nature (London) **517**, 64 (2015).

[38] G. Semeghini, M. Landini, P. Castilho, S. Roy, G. Spagnolli, A. Trenkwalder, M. Fattori, M. Inguscio, and G. Modugno, Measurement of the mobility edge for 3d Anderson localization, Nat. Phys. **11**, 554 (2015).

[39] M. Schreiber, S. S. Hodgman, P. Bordia, H. P. Lüschen, M. H. Fischer, R. Vosk, E. Altman, U. Schneider, and I. Bloch, Observation of many-body localization of interacting fermions in a quasi-random optical lattice, Science **349**, 842 (2015).

[40] J.-y. Choi, S. Hild, J. Zeiher, P. Schauß, A. Rubio-Abadal, T. Yefsah, V. Khemani, D. A. Huse, I. Bloch, and C. Gross, Exploring the many-body localization transition in two dimensions, Science **352**, 1547 (2016).

[41] P. Jurcevic, B. P. Lanyon, P. Hauke, C. Hempel, P. Zoller, R. Blatt, and C. F. Roos, Quasiparticle engineering and entanglement propagation in a quantum many-body system, Nature (London) **511**, 202 (2014).

[42] P. Richerme, Z.-X. Gong, A. Lee, C. Senko, J. Smith, M. Foss-Feig, S. Michalakis, and A. V. Gorshkov, and C. Monroe, Non-local propagation of correlations in quantum systems with long-range interactions, Nature (London) **511**, 198 (2014).

[43] J. Smith, A. Lee, P. Richerme, B. Neyenhuis, P. W. Hess, P. Hauke, M. Heyl, D. A. Huse, and C. Monroe, Many-body localization in a quantum simulator with programmable random disorder, Nat. Phys. **12**, 907 (2016).

[44] N. Trautmann and P. Hauke, Trapped-ion quantum simulation of excitation transport: Disordered, noisy, and long-range connected quantum networks, Phys. Rev. A **97**, 023606 (2018).

[45] S. Viciani, M. Lima, M. Bellini, and F. Caruso, Observation of Noise-Assisted Transport in an All-Optical Cavity-Based Network, Phys. Rev. Lett. **115**, 083601 (2015).

[46] D. N. Biggerstaff, R. Heilmann, A. A. Zecevik, M. Gräfe, M. A. Broome, A. Fedrizzi, S. Nolte, A. Szameit, A. G. White, and I. Kassal, Enhancing coherent transport in a photonic network using controllable decoherence, Nat. Commun. **7**, 11282 (2016).

[47] N. C. Harris, G. R. Steinbrecher, M. Prabhu, Y. Lahini, J. Mower, D. Bunandar, C. Chen, F. N. C. Wong, T. Baehr-Jones, M. Hochberg *et al.*, Quantum transport simulations in a programmable nanophotonic processor, Nat. Photonics **11**, 447 (2017).

[48] S. Mostame, P. Rebentrost, A. Eisfeld, A. J. Kerman, D. I. Tsomokos, and A. Aspuru-Guzik, Quantum simulator of an open quantum system using superconducting qubits: Exciton transport in photosynthetic complexes, New J. Phys. **14**, 105013 (2012).

[49] A. Potočnik, A. Bargerbos, F. A. Y. N. Schröder, S. A. Khan, M. C. Collodo, S. Gasparinetti, Y. Salathé, C. Creatore, C. Eichler, H. E Türeci *et al.*, Studying light-harvesting models with superconducting circuits, Nat. Commun. **9**, 904 (2018).

[50] C. F. Ockeloen, A. F. Tauschinsky, R. J. C. Spreeuw, and S. Whitlock, Detection of small atom numbers through image processing, Phys. Rev. A **82**, 061606(R) (2010).

[51] A. De Luca, B. L. Altshuler, V. E. Kravtsov, and A. Scardicchio, Anderson Localization on the Bethe Lattice: Nonergodicity of Extended States, Phys. Rev. Lett. **113**, 046806 (2014).